LA-UR -86-2974

Los Alamos National Laboratory is operated by the University of California for the United States Department of Energy under contract W-7405-ENG-36

LA-UR--86-2974

DE86 015318

TITLE THEORETICAL STUDY OF A HIGH-EXTRACTION EFFICIENCY UNDULATOR FOR A FREE-ELECTRON LASER OSCILLATOR

AUTHOR(S) H. Takeda, B. D. McVey, J. C. Goldstein

SUBMITTED TO Eighth International Free Electron Laser Conference
Glasgow, Scotland, September 1-5, 1986

DISCLAIMER

Los Alamos Los Alamos National Laboratory
Los Alamos, New Mexico 87545

Theoretical Study of a High-Extraction Efficiency Undulator for a Free-Electron Laser Oscillator*

Harunori Takeda, Brian D. McVey, John C. Goldstein

Los Alamos National Laboratory

MS E531, Los Alamos, NM 87545

Theoretical issues in designing a high-extraction efficiency undulator for a free-electron laser oscillator are discussed. Assuming that an undulator system consists of a prebuncher undulator and a main undulator separated by a drift, design criteria of the untapered prebuncher are studied. The main undulator is designed parabolically tapered in wave number from no taper to a 30% taper. A small signal gain is enhanced at the low taper section, and the large signal gain is enhanced at the high taper section. To optimize the operation of this prebuncher system, electron dynamics in phase space from the prebuncher to the main undulator is studied. To demonstrate the advantage of having the prebuncher, comparisons of the extraction efficiency and the gain are performed between the prebuncher system and the system with the prebuncher removed. The optimized prebuncher system is then tested for the sideband instability with more complex one-dimensional FEL codes that assume a finite electron pulse and a finite laser pulse length. The electron beam emittance requirement is studied using a three-dimensional FEL simulation code.

1. Introduction.

To design a high-extraction efficiency undulator, we explore a parabolically tapered undulator and a buncher device that almost doubles the efficiency and gain by prebunching

* Work performed under the auspices of the U.S. Dept. of Energy and supported by the U.S. Army Strategic Defense Command.

the electron micropulse into subpulses peaked at every laser wavelength. We discuss the design of the prebuncher, which is placed upstream from the undulator, and study effects using progressively more complex computer codes.

The prebuncher system described here, which is shown in fig. 1, is one variation of the multicomponent undulator developed by C. Shih and M. Caponi [1] and used in the TRW/Stanford experiment [2]. The main portion of the undulator is centered in the optical cavity. The prebuncher is placed at a certain distance from the end of the main undulator. Because the Gaussian optical mode expands from the waist at the center of the main undulator, the prebuncher requires a wider aperture than the aperture of the main undulator.

We derive a design with the required prebuncher undulator magnet gap to clear the optical wave and also find the prebuncher placement with respect to the main undulator. Then, we present the results of runs with one dimensional (1-D) simulation programs to calculate the efficiency and gain. To demonstrate the performance of the buncher concept, a comparison to the simple main-undulator-only configuration is made by removing the prebuncher.

When the intensity of the laser increases in the oscillator cavity such that there is about one synchrotron oscillation present while electrons pass through the main undulator, the effects of sidebands become significant. To show the performance of the compound undulator under the influence of sidebands, efficiency and gain are calculated with multi-pass simulation programs [3]. The electron and optical pulse shapes are included. The effects of electron-beam emittance on the efficiency and on the gain are calculated using a three dimensional FEL program [4]. FEL parameters used in the calculation are shown in table 1.

2. Gaussian mode requirement.

A simple formula relates the optical beam waist W_0 at $z = 0$ (the middle of the main undulator) and the beam radius $W(z)$ at any z through the Rayleigh range b_R :

$$W(z) \quad W_0 \sqrt{1 + \left(\frac{z}{b_R}\right)^2} \quad . \tag{1}$$

Assuming a 100 cm main undulator with b_R 49.5 cm , $W_0 = 0.15$ cm, and, assuming the prebuncher is placed 15 to 40 cm from the main undulator, the beam expands, at most, to a radius of 0.3 cm at the entrance to the prebuncher undulator. Including room for the wing of the Gaussian optical distribution, a prebuncher with a 0.6 cm radius aperture should be sufficient.

3. Prebuncher undulator gap, wavelength, and magnetic field.

The prebuncher undulator and the main undulator must satisfy the same resonance condition with identical values of dimensionless energy γ and laser wavelength λ_L. We assume that the magnet configuration is the Halbach type [5]: each block is 5 mm x 5 mm (block height: b 0.5 cm, block width: $w = 0.5$ cm) and the prebuncher is constructed with a vertical separation of $2h$ and a horizontal separation between successive centers of the blocks of λ_u 4, where λ_u is the undulator period. A remnant magnetic field B_r 8.72 kG is assumed.

The resonance condition and the Halbach formula are

$$k_u \quad \frac{k_L}{2\gamma^2}\left[1 + \frac{1}{2}\left(\frac{e}{mc^2}\frac{B_u}{k_u}\right)^2\right] , \tag{2}$$

and

$$B_u \quad \frac{8}{\pi} B_r e^{-k_u h} \sin\left[\frac{w}{2} k_u\right](1 \quad e^{-k_u b}) . \tag{3}$$

Solving the resonance condition, eq. (2), for B_u, we find

$$B_u \quad \left(\frac{k_u}{mc^2}\right)\sqrt{4\gamma^2\left(\frac{k_u}{k_L}\right) \quad 2} . \tag{4}$$

Substituting B_w from eq. (4) in eq. (3), we see that

$$k_u \sqrt{4\gamma^2 \left(\frac{k_u}{k_L}\right) - 2} = \frac{8}{\pi}\left(\frac{e}{mc^2}\right) B_r e^{-k_u h} \sin\left(\frac{u}{2} k_u\right)\left(1 - e^{-k_u b}\right). \qquad (5)$$

We can solve eq. (5) for the wave number k_u at a given h numerically. In fig. 2, the undulator wavelength λ_u is plotted against the half gap h. At $h = 0.6$ cm, λ_u is 3.048 cm, a 12% increase in wavelength over the main undulator, which has $h = 0.44$ cm and $\lambda_u = 2.73$ cm at the beginning. Also, the magnetic field B_w on axis at each half gap h is shown in fig. 2. It shows that at $h = 0.6$ cm, $B_w = 2.043$ kG. Using B_w and λ_w in the 1-D code, we optimize the distance where the prebunched electron beamlets are well trapped in the center of the receiving bucket of the main undulator.

4. Capture optimization using the one-dimensional FELP code [3].

The position at which the uniform prebuncher undulator should be placed is sensitive to the actual electron path length between the prebuncher and the main undulator. Because a real undulator has soft-edged fringe fields at both entrance and exit, the distance that gives the best efficiency as calculated with the program FELP, which assumes an abrupt cutoff of the field, may not exactly represent the optimum setting of the real experiment. However, when the distance is properly adjusted in the experiment, the capture efficiency and laser gain, as well as the capture process, should be correct to the extent that the one-dimensional model is valid.

We assume the energy of the electron beam to be $\gamma = 42.0$, full energy spread to be 1%, the electron beam current to be 150 A, and the length of the prebuncher (uniform undulator) to be $L_{bun} = 6$ cm. The optimization was performed assuming an intensity $1.3 \cdot 10^{11}$ W/cm^2 at the optical waist. The main undulator is assumed to have a parabolic taper with a wave number given by

$$k_w(z) = k_w(0)\left[1 - 0.3043\left(\frac{z}{L_{wig}}\right)^2\right]. \qquad (6)$$

The initial electron distribution in the longitudinal phase space is assumed to be uniform in phase. Defining a bunch capture distance L_{drift} as the separation between the downstream end of the prebuncher and the upstream end of the main undulator, the distance L_{drift} is optimized so that the highest efficiency is achieved for each bunch capture window. These windows are located at approximately every prebuncher period; however, because the phase shift of the laser depends on the bunch capture distance, the windows are not spaced exactly at every prebuncher period. Numerical simulations show that the capture windows open at capture distances, for example, L_{drift} = 6.99 *cm*, 10.5 *cm*, 17.34 *cm*, 21.07 *cm*, 24.5 *cm*, and 31.52 *cm*. This optimization is discussed below.

Consider the case with L_{drift} = 31.52 *cm*. The right half of fig. 3 shows the electron phase-space distributions without prebuncher at 16 *cm* from the entrance of the main undulator and at its exit. The electrons are compressed in phase, but many of them are near to, or outside of, the bucket boundary (separatrix). Only 19% of them are within the bucket at the exit. The efficiency and the gain are 6.618% and 3.7%, respectively. Also shown in the left half of fig. 3 are the prebuncher compressed electron distribution near the entrance to the main undulator and the distribution at the exit of the main undulator. At the exit, 41% of the electrons are within the bucket. The efficiency and the gain are nearly doubled, to 11.71% and 6.5%, respectively, by the presence of the prebuncher.

Figure 4 shows the efficiency and gain plotted against L_{drift}. The efficiency and gain show that we have a better performance at longer L_{drift}, but over-bunching eventually degrades the performance because over-bunched electrons have a larger phase spread in the accepting bucket. For a prebuncher with L_{bun} = 6 *cm*, the optimum is at L_{drift} = 31.52 *cm*.

5. Effect of varying the length of the prebuncher undulator.

The prebuncher length L_{bun} is limited by the condition that the energy width of the prebunched electron micropulse should not exceed the minimum bucket height in the main

undulator. However, this is not clear cut because the synchrotron motion of electrons within the bucket transforms phase-angle spread to energy spread.

The main undulator, tapered parabolically with wave number, is also tapered with the on-axis magnetic field. Knowing both the the wave number taper $\frac{dk_w}{dz}$ and the on-axis magnetic field taper $\frac{dB_w}{dz}$, the resonant angle Ψ_R can be expressed as an implicit function of z through the variables B_w and k_w (assuming the laser phase change is insignificant):

$$\sin\Psi_R = \frac{\tilde{a}_w}{2a_L k_w^2}\left\{\left(\frac{1}{2a_w^2}+\frac{3}{2}\right)\frac{dk_w}{dz} - \frac{k_w}{B_w}\frac{dB_w}{dz}\right\}. \tag{7}$$

where $\tilde{a}_L$ and a_w represent the dimensionless rms vector potentials for the laser and undulator, respectively.

Differentiating eq. (3) with respect to z, we have

$$\frac{dB_w}{dz} = \frac{8}{\pi}B_r e^{-k_w h}\frac{dk_w}{dz} \cdot\left[(1-e^{-k_w b})\left\{h\sin\left(\frac{wk_w}{2}\right)+\frac{w}{2}\cos\left(\frac{wk_w}{2}\right)\right\}+be^{-k_w b}\sin\left(\frac{wk_w}{2}\right)\right]. \tag{8}$$

Differentiating eq. (6) with respect to z, we find

$$\frac{dk_w}{dz} = k_w(0) = 0.6086\left(\frac{z}{L_{w\text{-}tg}^2}\right). \tag{9}$$

From eqs. (7), (8), (9), and (3), one can calculate Ψ_R as a function of z. The result is shown in fig. 5 with the profiles of magnetic field, wavelength, and bucket half height at laser intensity 10^{11} W/cm^2. The parabolic taper starts with zero resonant angle and smoothly increases to 40.64°. Because the changes in $\tilde{a}_L$ and $\tilde{a}_w$ are small over the undulator, the bucket height is a minimum at the maximum resonant angle where the relative bucket half height is (2.53%) as compared to 6.06% at $\Psi_R = 0°$. The half-energy spreads of the electron microbunch near the entrance of the main undulator are calculated with the code FELP at the drift distance 24.5 *cm*. The spreads are 2.3%, 2.4%, and 2.6% for prebuncher lengths L_{bun} of 4.5 *cm*, 7.5 *cm*, and 9.0 *cm*, respectively. The slightly larger energy spread, which is induced by the longer prebuncher compared to the bucket

half height 2.53% at the end of the main undulator, reduces both efficiency and gain. Calculated efficiency and gain as functions of the prebuncher length L_{bun} are shown in fig. 6. Both the efficiency and gain peak at $L_{bun} = 7.5\ cm$, but variations of 0.5% in either of them are not significant.

6. Spectra of the extraction efficiency and the small and the large signal gains.

The prebuncher with $L_{drift} = 31.52\ cm$ and $L_{bun} = 6.0\ cm$ has a well-peaked small signal gain (~30%) near 10.1 μm. The large signal efficiency and gain also are peaked near the design wavelength 10.1 μm (fig. 7).

When the prebuncher is removed, the small signal gain peaks at the design wavelength, but it is ~13% less than with the prebuncher. The bandwidths as seen in fig. 7 are larger. For the large signal efficiency and gain, the spectra are much broader than with the prebuncher (fig. 8). For both efficiency and gain, the magnitudes of the peaks are about half those found with the prebuncher installed.

7. Comparison of the buncher undulator with a parabolic undulator of equal total length.

Instead of having a spacing $L_{drift} = 31.52\ cm$ and a 6-cm prebuncher, a parabolic undulator with the same total length of the undulator system without the prebuncher is tested for comparison. Assuming the parabolic undulator's length to be 137.52 cm and its half gap to be 0.44 cm, the efficiency and gain are found to be 8.52% and 3.2%, respectively. These percentages are much smaller than those of the buncher-undulator system.

8. Study of sideband effect using one-dimensional FEL codes [3].

Using one-dimensional FEL codes that assume a parabolic electron beam pulse (FWHM ~ 14 $psec$), the efficiency and gain are tested for the prebuncher undulator system

in multiple pass oscillator simulations. The desynchronism is assumed to be zero. The micropulse peak current is assumed to be 150 A.

Figure 9 compares the extraction efficiency of the prebuncher system to the extraction efficiency with the prebuncher removed. With the presence of the prebuncher, the efficiency rose to 9% by Pass 150. Because of the finite pulse effect, the efficiency at the peak is smaller by 23% than the FELP calculation. At Pass 200, the efficiency dropped to ~5%. The gain peaks at 26% at Pass 70, but it drops sharply to 5% by Pass 150, where the intensity and the extraction efficiency saturate. It then stays nearly constant.

For the system without prebuncher, the efficiency rises to ~5% by Pass 250; it then decreases to ~4% and stays nearly constant. As a result, the prebuncher system has approximately 1% higher efficiency when sidebands are fully developed in both systems.

Figure 10 shows spectra of electric field at different pass numbers. At Pass 150, only the resonant peak is present. However, at Pass 195, sidebands start growing at both sides of the peak and the drop in efficiency is observed (fig. 9). After 255 passes, the sideband with the longer wavelength has a larger field strength. We also see the next generation of sidebands starting to grow.

Additional 1-D finite pulse calculations yielded the following results: (1) the width of the desynchronism curve was found to be about 20 μm, and (2) the maximum extraction efficiency with an optical cavity having multilayer dielectric mirrors, whose reflectivity and phase shift as functions of frequency were included in the calculation, increased to about 9%. The mirror reflectivities prevented the development of sidebands in this latter result.

9. Study of beam emittance effect using three-dimensional program FELEX[4].

The effect of the emittance of the electron beam was studied using a 3-D program. Figure 11 shows the efficiency and the small and large signal gains as functions of the emittance for two types of initial electron transverse phase-space distributions. Although the uniform distribution is superior to the Gaussian distribution, both the efficiency and

the gain decrease rapidly as the emittance increases. To achieve a high efficiency and high gain, it is necessary to have a high-quality electron beam, preferably $\epsilon \leq 1\pi\ mm \cdot mrad$.

References

[1] C. Shih and M.Z. Caponi, "An Optimized Multicomponent Wiggler Design for a Free Electron Laser Oscillator," IEEE J. Quantum Electron., Vol. QE-19, 369-373, 1983.

[2] G.R. Neil, J.A. Edighoffer, S.W. Fornaca, C.E. Hess, T.I. Smith, and H.A. Schwettman, "The TRW/Stanford Tapered Wiggler Oscillator," Nucl. Instr. and Meth. in Phys. Res., A237, 199-202, 1985.

[3] FELP is a one-dimensional free-electron laser code written by B.D. McVey, which runs either in the continuous-beam mode or in the pulsed-beam mode. See also J.C. Goldstein, "Evolution of long pulses in a tapered wiggler free-electron laser," in Free Electron Generators of Coherent Radiation, C.A. Brau, S.F. Jacobs, and M.O. Scully, eds., SPIE 453, 2, 1984.

[4] FELEX is a three-dimensional free-electron laser code written by B.D. McVey; "Three-Dimensional Simulations of Free-Electron Laser Physics," to be published in the proceedings of the 1985 Free-Electron Laser Conference in Nucl. Instr. and Meth. in Phys. Res., 1986.

[5] K. Halbach, Nucl. Instr. and Meth. 187 (1981), 109.

Table 1. FEL parameters with prebuncher

Electron Beam:	
I	150 A
γ	42
$\frac{\Delta\gamma}{\gamma}$	1%
ϵ	$1\pi\ mm \cdot mrad$
Main Undulator:	
L_w	100 cm
$B_w(0)$	3 kG
$\lambda_u(0)$	2.74 cm
Prebuncher:	
L_{bun}	6 cm
B_{bun}	2.043 kG
λ_{bun}	3.048 cm
L_{drift}	31.52 cm
Optical:	
λ_L	10.1 μm
b_E	49.5 cm

Figure Captions

Fig. 1. A prebuncher with a few periods is placed upstream of a tapered undulator.

Fig. 2. Prebuncher period and magnetic field on axis are parametrized with the half gap.

Fig. 3. The electron distribution near the entrance and at the exit of the main undulator without prebuncher (right half) and with prebuncher (left half).
Z coordinate origin is at the center of the main undulator.

Fig. 4. Extraction efficiency and gain depend on the position of the capture window, which is determined by the capture distance.

Fig. 5. The main undulator magnetic field, wave number, bucket half height, and corresponding resonant angle profiles.

Fig. 6. The gain and efficiency depend little on the prebuncher length when the main undulator is parabolically tapered.

Fig. 7. Spectra of small signal gain, extraction efficiency, and large signal gain for the prebuncher system. They show narrower bandwidths and higher performance than without the prebuncher.

Fig. 8. Spectra of small signal gain, extraction efficiency, and large signal gain for a parabolic undulator only. They have broad bandwidths.

Fig. 9. Comparison of extraction efficiencies with multiple-pass, finite-pulse, 1-D calculations. Initial rise before sideband effect shows a large difference between the systems with and without prebuncher.

Fig. 10. Electric field spectra. Near 200 passes, sidebands are rising, clearly reducing the amplitude of the main peak.

Fig. 11. The emittance rapidly degrades the performance of the system. Extraction efficiency and gain decrease for either uniform or Gaussian transverse electron distributions.

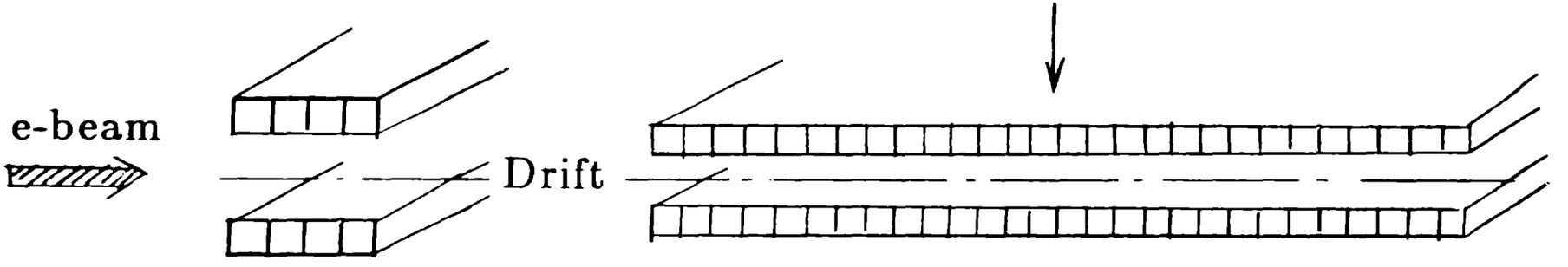

Prebuncher

Tapered Undulator

Prebuncher wavelength

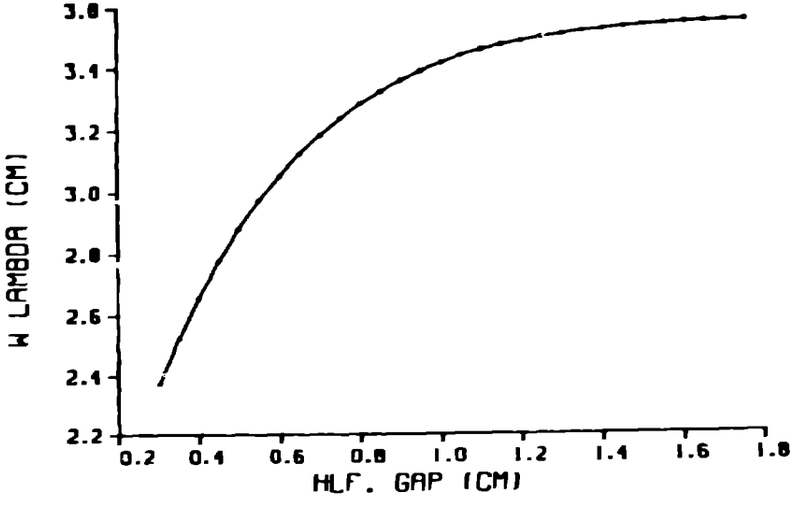

Prebuncher B field

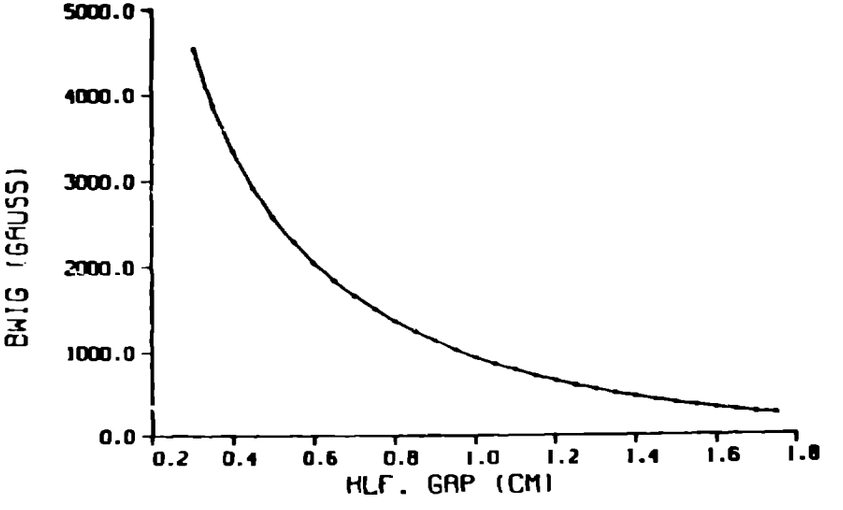

Prebuncher + Undulator

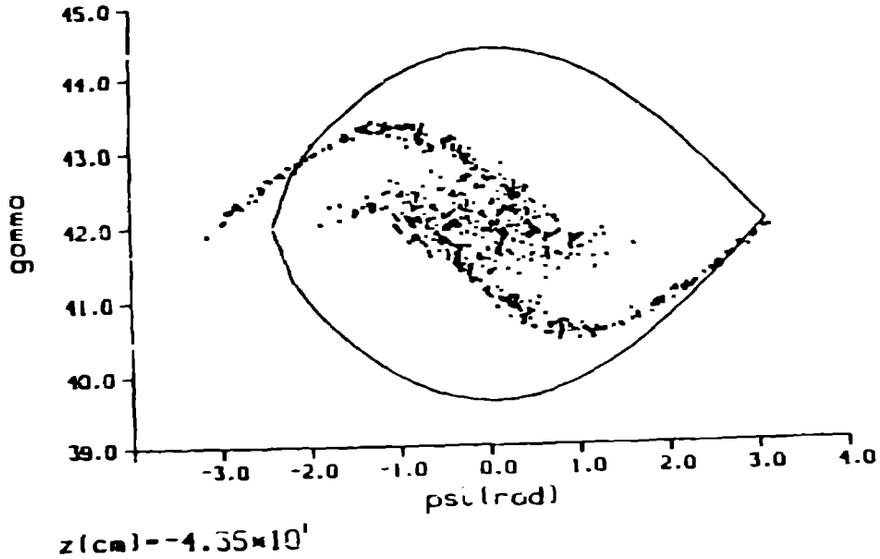

z(cm)=-4.35×10¹

Undulator – only

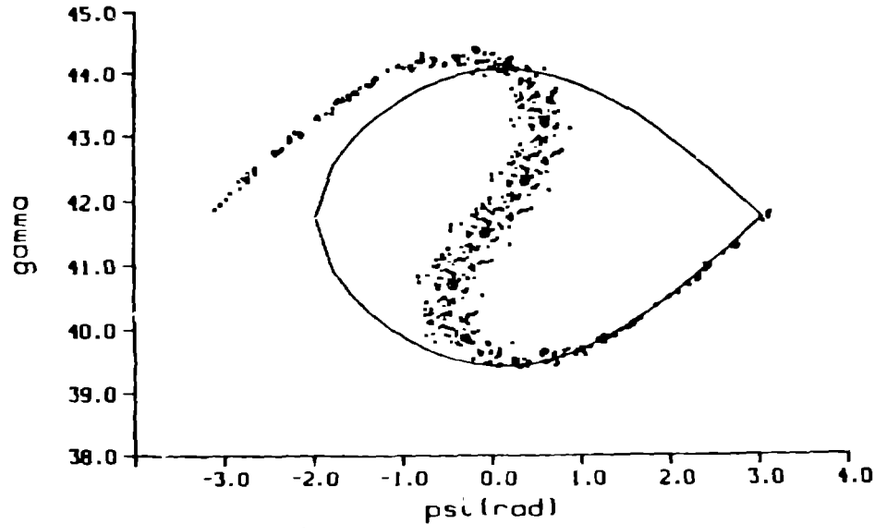

z(cm)=-3.40×10¹

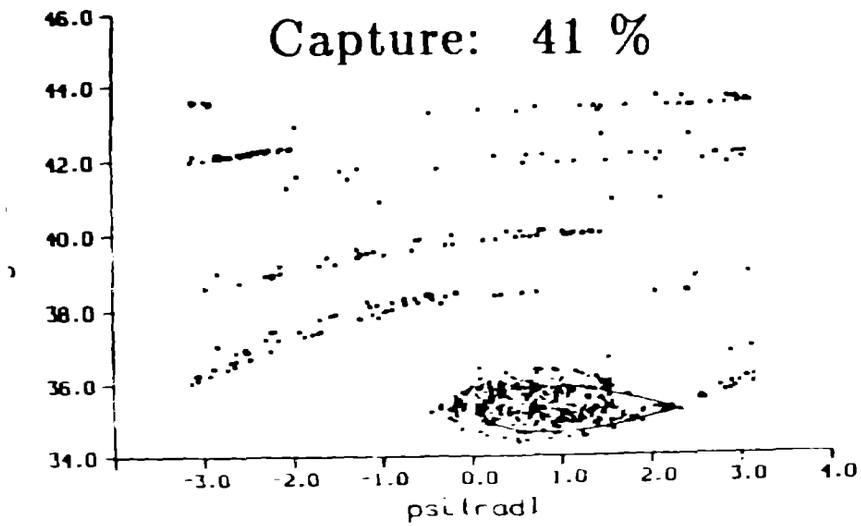

z(cm)= 5.00×10¹

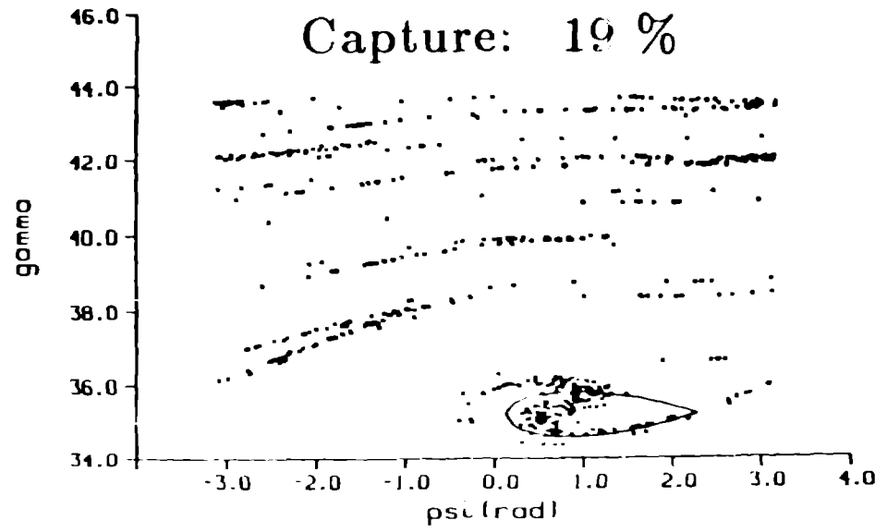

z(cm)= 5.00×10¹

Efficiency

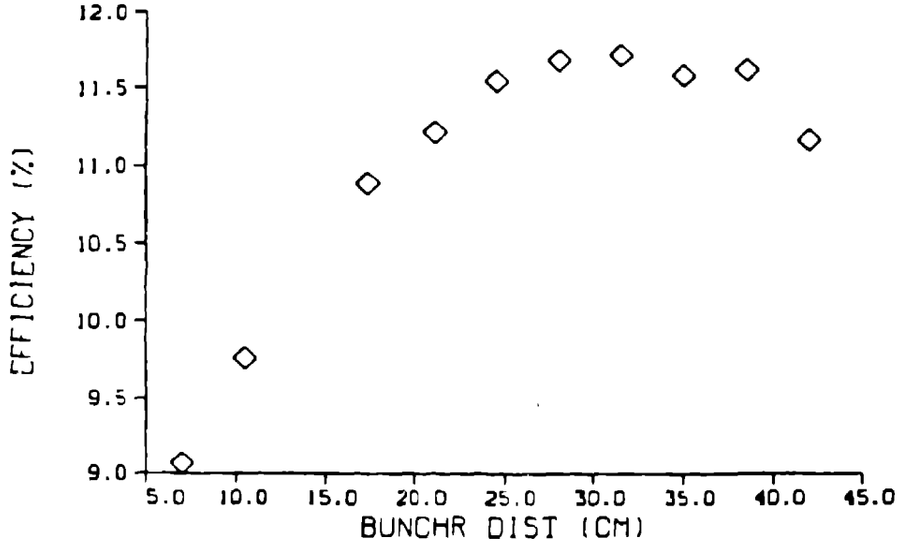

Gain

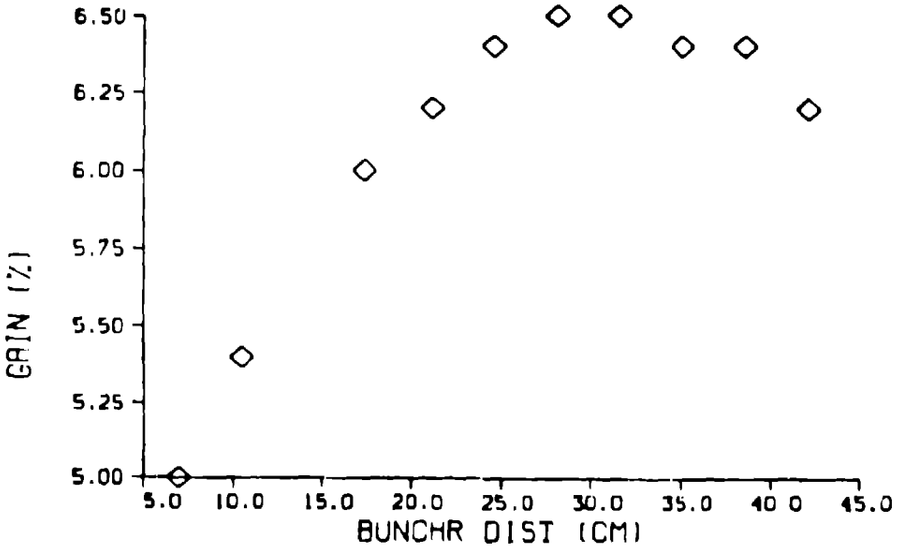

B field

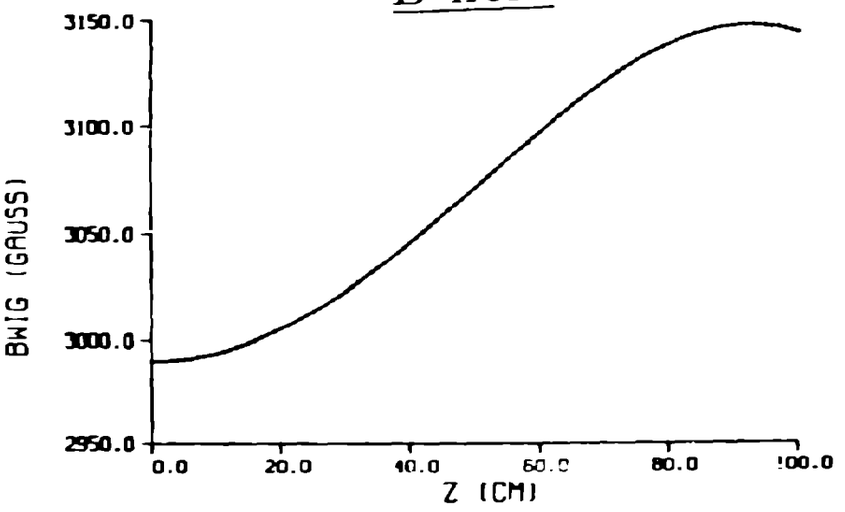

Wavelength

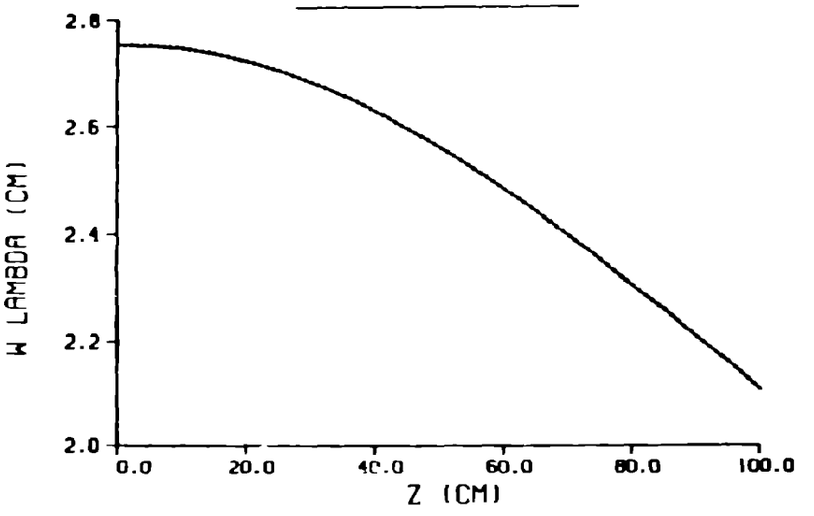

Half bucket height

(10^{11} W/cm^2)

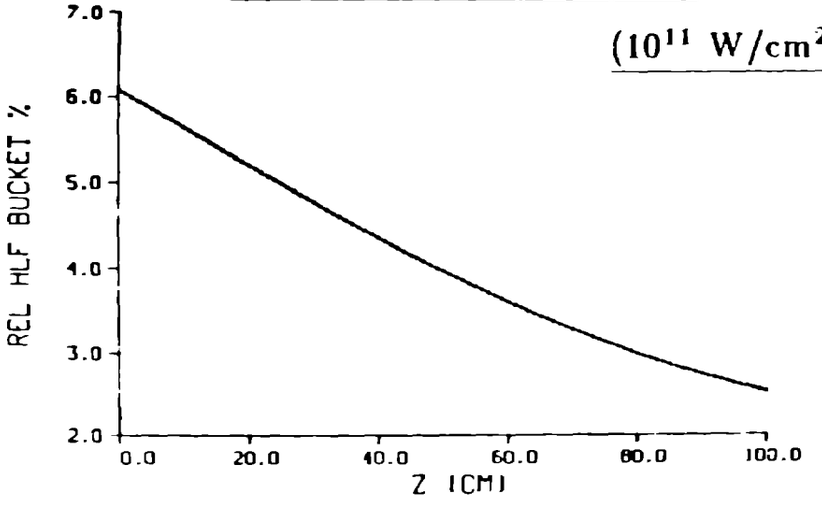

Resonant angle

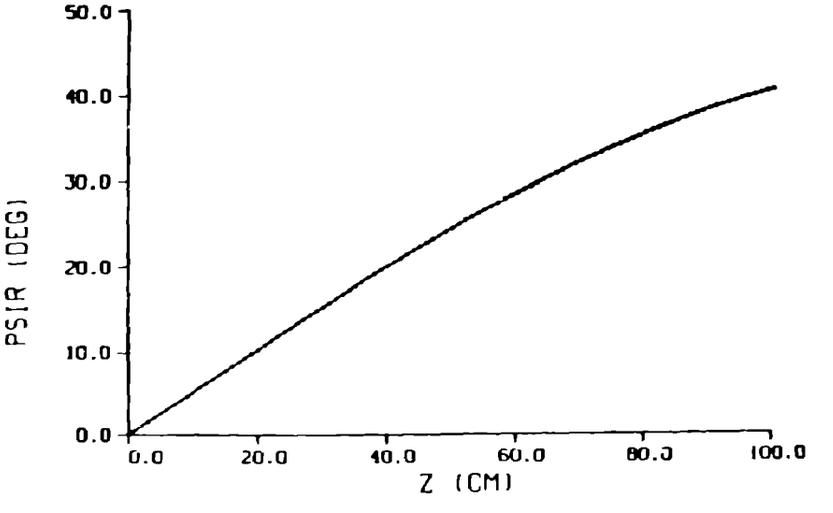

Efficiency

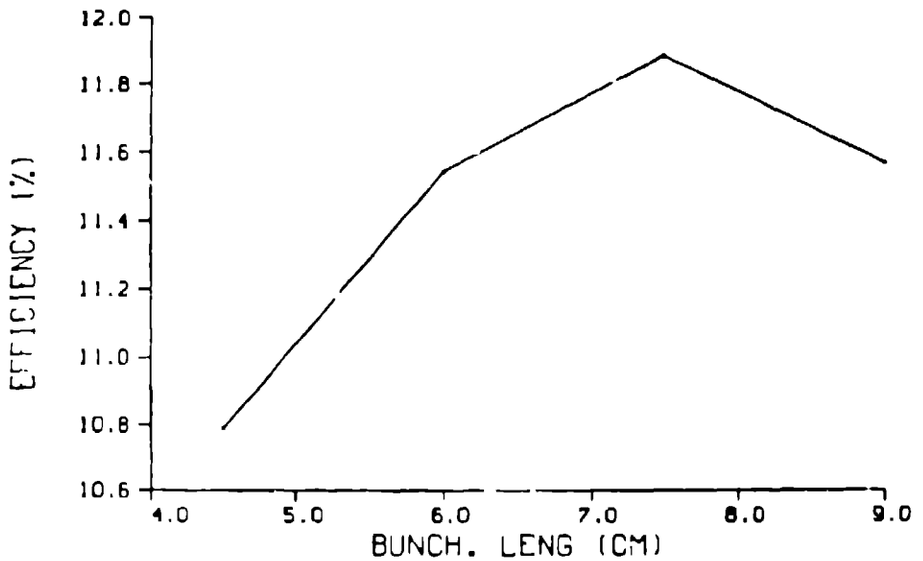

Gain

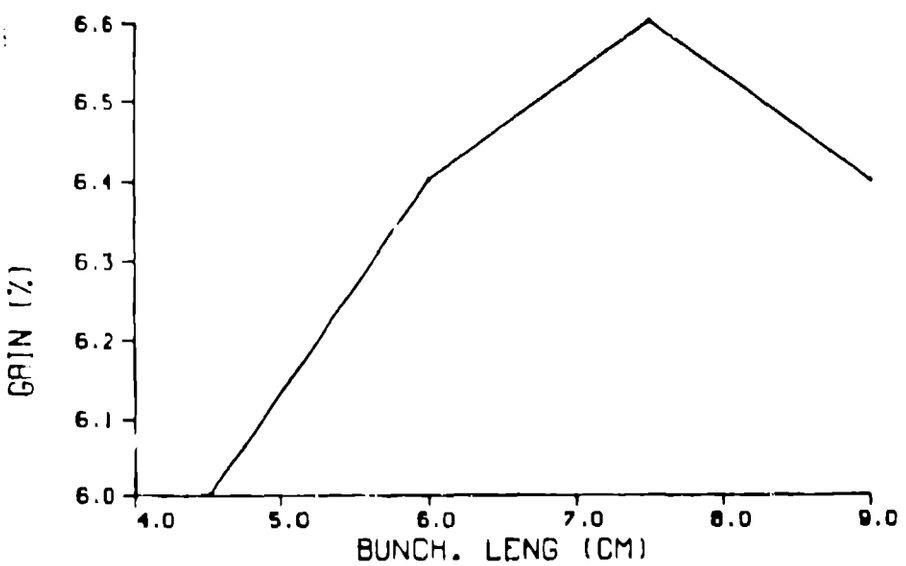

Small signal gain

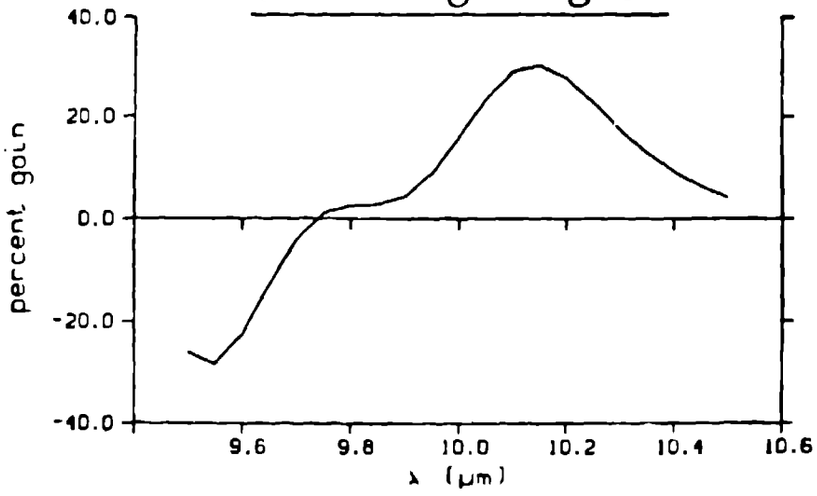

optical power density (w/cm^2) = 1.00×10^6

Extraction efficiency

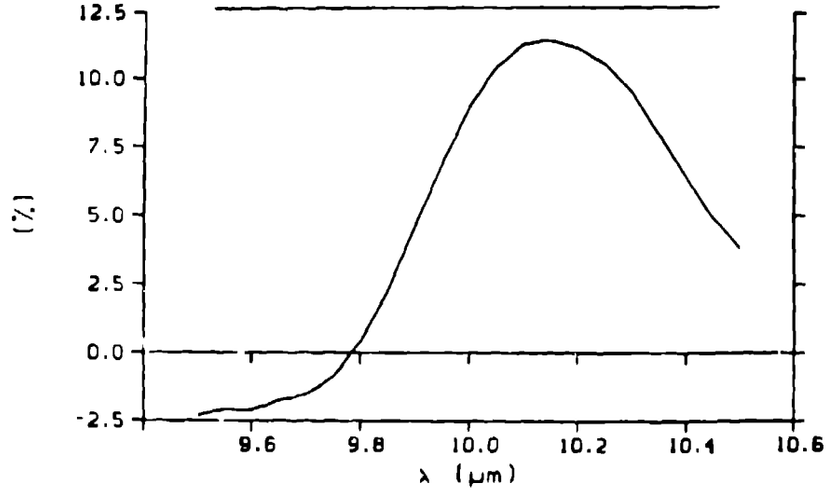

Large signal gain

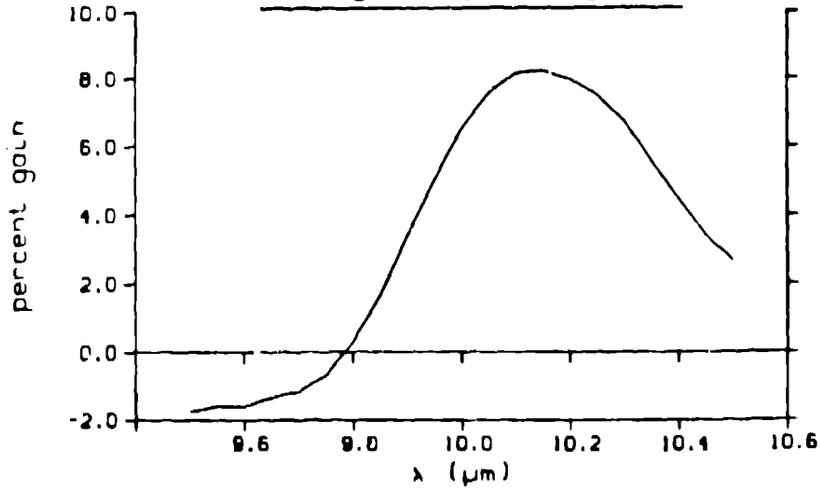

Small signal gain

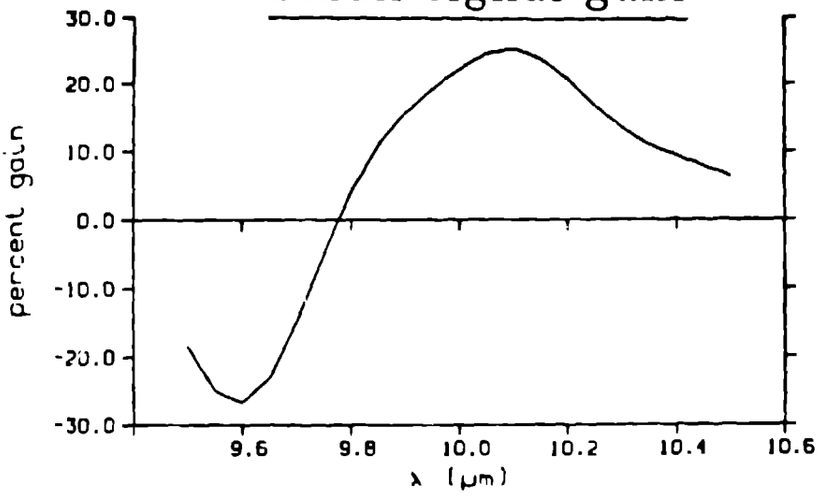

optical power density (w/cm^2) = 1.00×10^6

Extraction efficiency

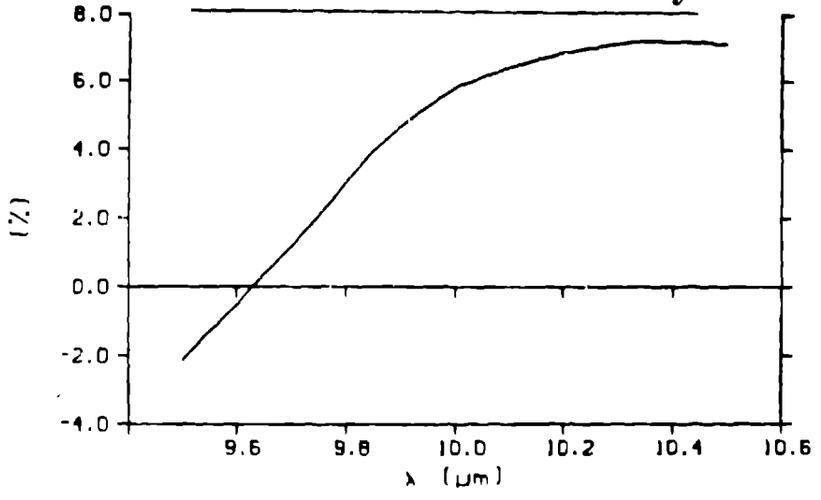

Large signal gain

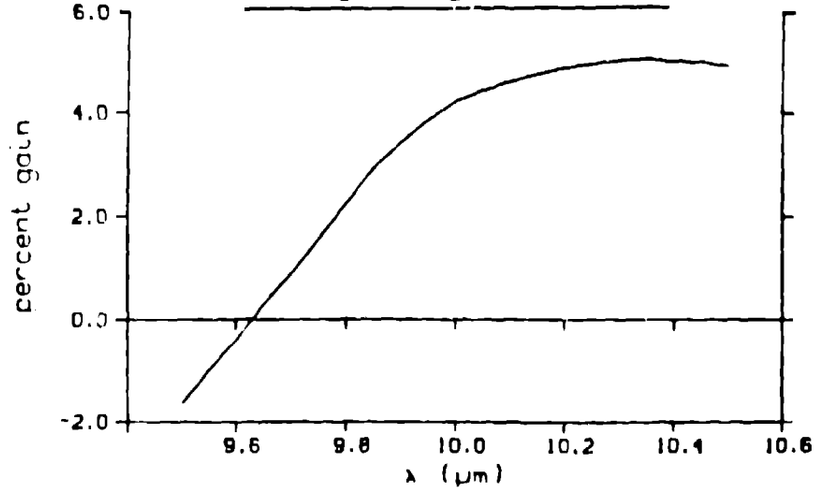

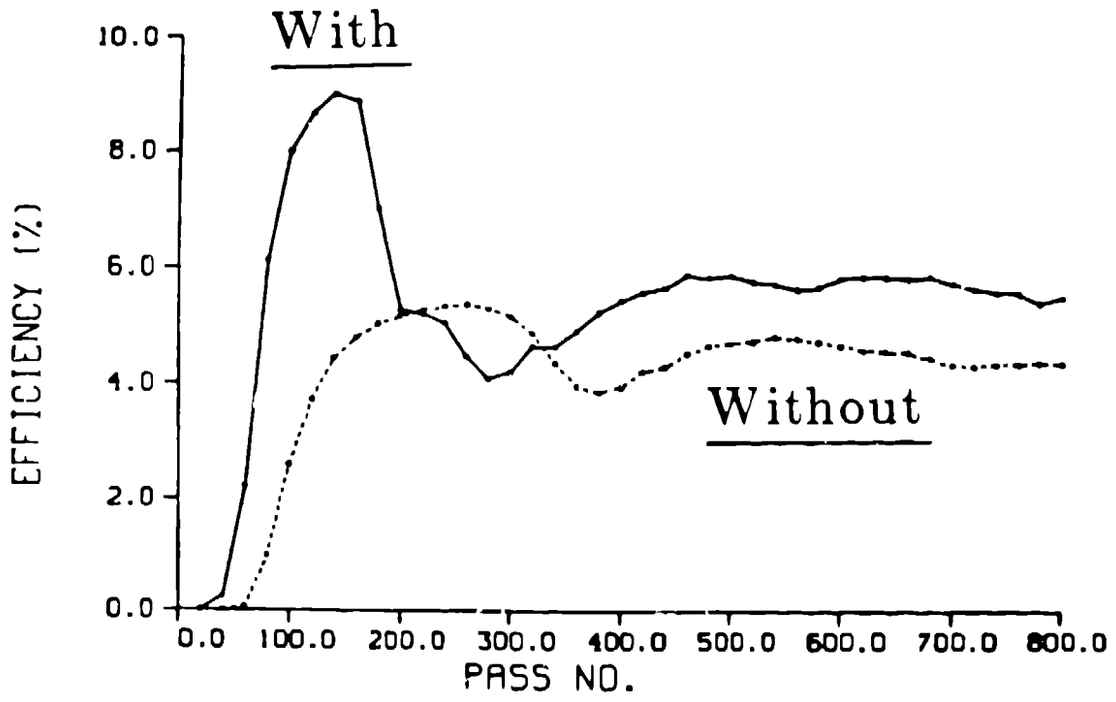
With
Without
EFFICIENCY (%)
10.0
8.0
6.0
4.0
2.0
0.0
0.0
100.0
200.0
300.0
400.0
500.0
600.0
700.0
800.0
PASS NO.

Electric field spectrum

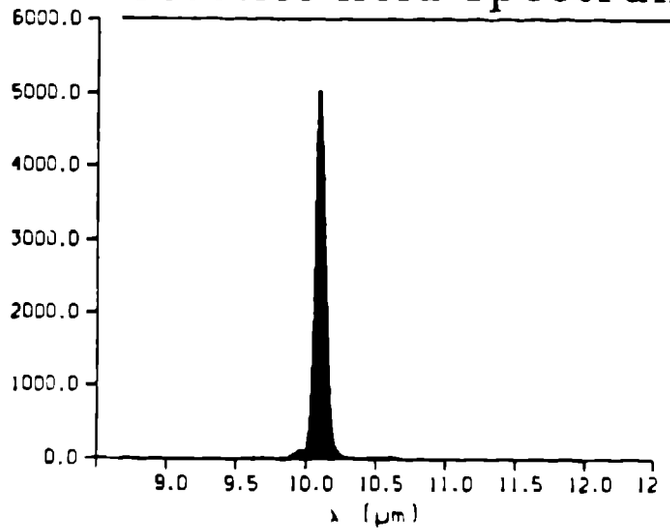

poss number=150

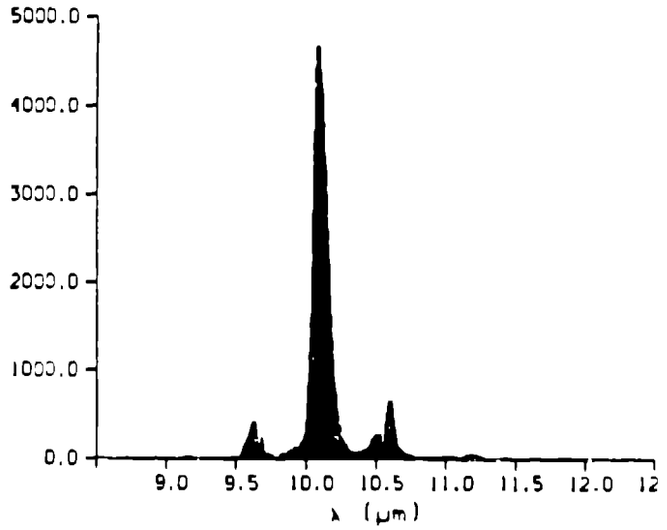

poss number=195

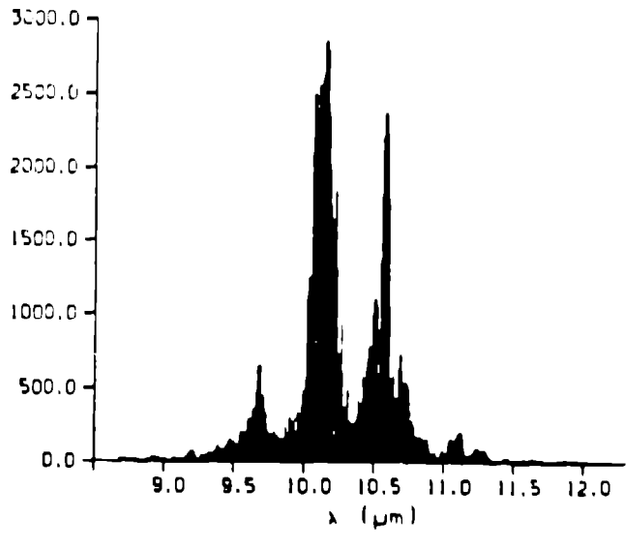

poss number=255

Small signal gain

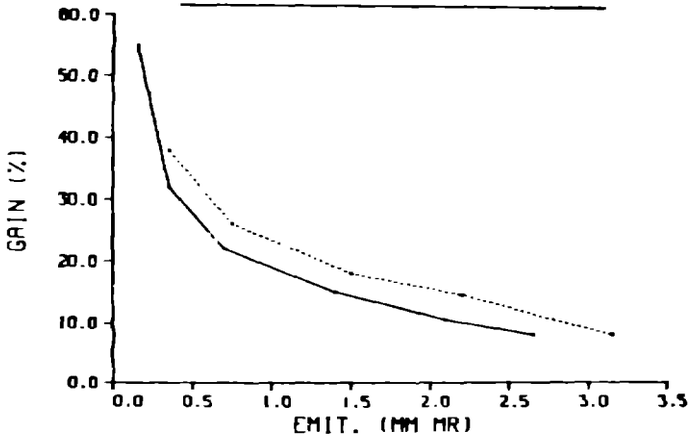

Transverse phase space

——— Gaussian

..... Uniform

Large signal gain

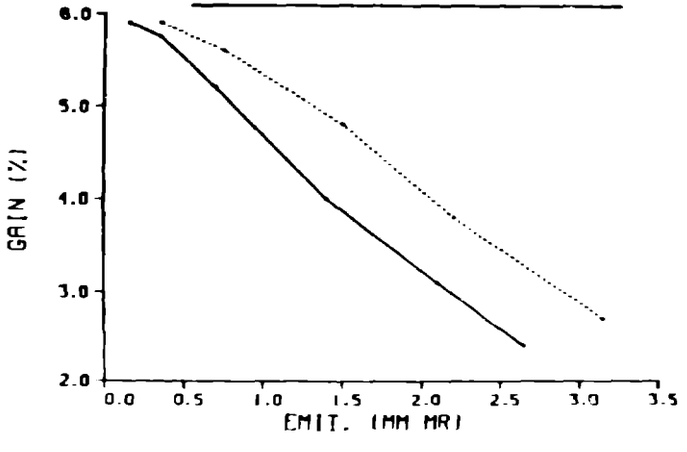

Extraction efficiency